Available at www.sciencedirect.com

ScienceDirect

journal homepage: www.elsevier.com/locate/he

Nanoscale composition modulations in $Mg_yTi_{1-y}H_x$ thin film alloys for hydrogen storage

A. Baldi[a,*], R. Gremaud[a,1], D.M. Borsa[a,2], C.P. Baldé[b], A.M.J. van der Eerden[b], G.L. Kruijtzer[c], P.E. de Jongh[b], B. Dam[a], R. Griessen[a]

[a]Department of Physics and Astronomy, VU University Amsterdam, De Boelelaan 1081, 1081 HV Amsterdam, The Netherlands
[b]Department of Chemistry, Utrecht University, Sorbonnelaan 16, 3584 CA Utrecht, The Netherlands
[c]Debye Institute for NanoMaterials Science, Utrecht University, P.O. Box 80.000, 3508 TA Utrecht, The Netherlands

ARTICLE INFO

Article history:
Received 21 October 2008
Received in revised form
22 November 2008
Accepted 24 November 2008
Available online 3 January 2009

Keywords:
Hydrogen storage
Immiscible alloys
Chemical short-range order

ABSTRACT

A detailed structural analysis of Mg–Ti–H thin films reveals the presence of a chemically partially segregated but structurally coherent metastable phase. By combining X-Ray Diffraction and Extended X-ray Absorption Fine Structure (EXAFS) spectroscopy on $Mg_yTi_{1-y}H_x$ thin films we find non-zero Chemical Short-Range Order (CSRO) parameters for all the compositions measured. Despite the positive enthalpy of mixing of Mg and Ti the degree of ordering does not increase upon loading and unloading with hydrogen. The robustness of this system and the fast and reversible kinetics of hydrogen loading and unloading are caused by the formation of nanoscale compositional modulations in the intermetallic alloy. This microstructure is responsible for the exceptional properties of $Mg_yTi_{1-y}H_x$ thin films. It also shows that reversible metastable metal-hydrides offer new possibilities for hydrogen storage, beyond the limits imposed by thermodynamic equilibrium.

1. Introduction

The Mg–Ti–H system is currently attracting a lot of attention, with potential applications in very different fields. Niessen et al. [1] proposed the use of Mg–Ti thin films as high-capacity hydrogen storage materials for batteries. By means of electrochemical loading of $Mg_{0.8}Ti_{0.2}$ thin films they found a gravimetrical storage capacity of 6.53 wt% H: ~4 times higher than the commercially available NiMH batteries. In our group we demonstrated the possibility of gas loading of Pd-capped Mg_yTi_{1-y} thin films. These films, when exposed to hydrogen gas exhibit fast and reversible transitions from the metallic to the hydrogenated state. The Ti doping of Mg greatly enhances the kinetics of hydrogen uptake and release. A 65 nm thick film of $Mg_{0.7}Ti_{0.3}$, exposed to 5% H_2 in Ar at room temperature, hydrogenates completely in ~10 s; if it is then exposed to 20% O_2 in Ar, it fully desorbs in less than 3 min, returning to its original metallic state [2]. The role of Ti is to favor the formation of a face-centered cubic hydride phase of $Mg_yTi_{1-y}H_x$ (for $y < 0.87$ [3]) instead of the tetragonal MgH_2-like phase.

The hydrogenation of Mg_yTi_{1-y} thin films is also accompanied by dramatic optical changes, which make them suitable for application as hydrogen sensors [4] and smart coating for solar collectors [5]: when exposed to hydrogen gas, they exhibit fast and reversible (>100 cycles) optical transitions

* *Corresponding author.*
E-mail address: abaldi@few.vu.nl (A. Baldi).
[1] Present address: Empa, Ueberlandstrasse 129, CH-8600 Dübendorf, Switzerland.
[2] Present address: ECN Solar Energy, Westerduinweg 3NL 1755 LE Petten, The Netherlands.

0360-3199/$ – see front matter © 2008 International Association for Hydrogen Energy. Published by Elsevier Ltd. All rights reserved.
doi:10.1016/j.ijhydene.2008.11.090

from a shiny metallic state to a black, strongly light-absorbing, hydrogenated state [2].

In order to explain these properties and eventually to control and tailor them, we need to fully understand the microstructure of these materials. Mg and Ti are immiscible elements in thermodynamic equilibrium, as their enthalpy of mixing, ΔH_{mix}, is positive. For a $Mg_{0.50}Ti_{0.50}$ mixture, $\Delta H_{mix} \approx 20$ kJ/g-atom [6]. The synthesis of Mg–Ti alloys has nevertheless been achieved both in bulk and in thin films via non-equilibrium processes such as physical vapor deposition [7], e-beam deposition [1,8], sputtering [2,9,3] and mechanical alloying [10].

In a previous work we measured the optical, structural and electrical properties of $Mg_yTi_{1-y}H_x$ ($y = 0.7$, 0.8 and 0.9) thin films [3]. The XRD patterns and the TEM plane-view and cross-sectional images of the as-deposited metallic films showed crystalline hexagonal close-packed structures for all compositions, with an almost perfect Vegard's law [11] dependence of the average lattice spacing. This suggests at first sight a microstructure made of a single-phase supersaturated solid solution of randomly dispersed Mg and Ti atoms. However, the optical and electrical properties of these films hint to a more complex microstructure, consisting of partially segregated Mg-rich and Ti-rich nanosized domains, within large structurally coherent grains [3].

Standard X-ray diffraction techniques are, however, not sufficient to prove the validity of this model [12]: nanoscale short-range deviations from a random solid solution would also produce a Vegard's law dependence, provided that the coherence is maintained [13]. Such deviations can arise because of incipient phase separation during the synthesis of the alloy.

In the present work we study the local atomic ordering in sputtered $Mg_yTi_{1-y}H_x$ thin film by means of X-Ray Diffraction (XRD), Extended X-ray Absorption Fine Structure (EXAFS) spectroscopy and X-Ray Absorption Near Edge Structure (XANES) spectroscopy. EXAFS spectra of Mg_yTi_{1-y} thin films with various compositions are measured both for the as-deposited state and for the samples after one cycle of loading and unloading with hydrogen. XANES spectra are measured continuously during hydrogenation and de-hydrogenation of the films, in order to follow the phase transitions that occur during these processes.

From the analysis of the EXAFS data of Mg_yTi_{1-y} thin films with different compositions we derive the coordination shells for Ti and the corresponding chemical short-range order parameter, s. All the measured compositions have positive s values, indicating that partial chemical segregation has occurred during the film deposition. The degree of ordering is maintained upon cycling with hydrogen. Such reversibility is particularly unexpected considering the positive enthalpy of mixing of Ti and Mg and the hydrogen-induced phase separation observed in many other Mg-based binary systems [14,15].

Similar metastable structures with short-range compositional modulations can in general be obtained in bulk via non-equilibrium processes such as mechanical alloying and liquid quenching [12]. A metastable Mg_7TiH_x powder with gravimetric hydrogen storage capacity of 5.5 wt% has been prepared by high-pressure synthesis [16]. However, the microstructure of this compound, an atomically ordered Ca_7Ge-like superstructure, is very different from the one found in Mg_yTi_{1-y} thin films. High-pressure Mg_7TiH_x releases 4.7 wt% of hydrogen at 332 °C decomposing in Mg and $TiH_{1.9}$, but the process is not reversible, although several attempts to produce destabilized bulk Mg–Ti–H alloys, with reversible hydrogen sorption properties, are currently under way [17]. Our study on thermodynamically metastable but reversible Mg_yTi_{1-y} thin film alloys shows the existence of a new class of hydrogen storage system that is not restricted by conventional thermodynamic equilibrium considerations and has excellent kinetic properties.

2. Experimental section

Mg_yTi_{1-y} films are deposited in an UHV system (base pressure $= 10^{-8}$ mbar) by DC/RF magnetron co-sputtering of Mg and Ti targets in argon atmosphere, on glassy carbon SIGRADUR® substrates of 100 μm thickness, kept at room temperature. The films are covered with 20 nm of Pd to prevent oxidation and promote hydrogen dissociation. Typical deposition rates are 0.22 nm/s for Mg at 150 W (RF), 0.02–0.18 nm/s for Ti at 60–400 W (DC) and 0.11 nm/s for Pd at 50 W (DC). In order to obtain a homogenous composition the substrates are continuously rotated during sputtering. The characteristics of the films used in this work are given in Table 1.

Film composition and thickness are measured *ex-situ* by Rutherford Backscattering Spectrometry (RBS) and profilometry, respectively. X-ray diffraction patterns are measured in a θ–2θ configuration, with a Bruker D8 Discover diffractometer equipped with a two-dimensional detector for real-time data collection over a large area with high sensitivity and low background. A typical diffraction pattern is recorded in 1 h. A beryllium dome allows *in-situ* diffraction measurements during hydrogenation of the films at room temperature in a hydrogen pressure of 10^5 Pa.

Titanium K-edge (4966 eV) EXAFS spectra are recorded at beamline E4 of the DORIS III storage ring at the Deutsches Elektronen-Synchrotron (DESY), Hamburg. The beamline is equipped with a Si [11] double-crystal monochromator, which is detuned to 60% of the Bragg peak intensity to suppress higher harmonics, and two mirrors: an Au coated toroidal mirror and a plane Ni mirror for optimum higher order harmonics reduction at the energies used. Samples are measured in transmission at room temperature, in He flow (for as-deposited and de-hydrogenated films) or in a 5% H_2/He

Table 1 – Alloy composition, film thickness and deposition rates of the samples used.

Sample Number	Composition	Thickness [nm]	Mg rate [nm/s]	Ti rate [nm/s]
1	$Mg_{0.53}Ti_{0.47}$	250	0.22	0.18
2	$Mg_{0.59}Ti_{0.41}$	310	0.22	0.13
3	$Mg_{0.70}Ti_{0.30}$	360	0.22	0.09
3a	$Mg_{0.72}Ti_{0.28}$	2000	0.36	0.12
4	$Mg_{0.81}Ti_{0.19}$	410	0.22	0.05
5	$Mg_{0.90}Ti_{0.10}$	460	0.22	0.02

mixture flow (for hydrogenated films). XANES spectra are recorded while loading the films in 5% H_2/He mixture at room temperature and unloading in 20% O_2/He mixture between room temperature and 100 °C, depending on film's composition. In each measurement a pile of 8–12 films, with the same composition and deposited in the same run, are inserted into the beam, in order to obtain sufficient absorption and a high signal to noise ratio. Three consecutive ionization chambers allow to simultaneously measure the absorption spectra of both the sample and a reference Ti foil.

In order to calibrate the Ti–Ti and Ti–Mg references we use a 5 μm thick Ti foil (99.99%) and $TiAl_3$ (99.5%) powder, respectively.

The EXAFS data are extracted from the measured absorption spectra with XDAP [18]. At least five scans for each sample are averaged together. The edge-energy is determined from the maximum of the first derivative of the spectrum and calibrated with the reference Ti foil. A smooth atomic background function, represented by a cubic spline, is used to extract the EXAFS oscillation from the absorption spectrum [19]. The obtained data are normalized by the background height 50 eV after the edge. Experimental data are fitted in k-space with k^3 weighting, using the difference file technique in real space [20].

3. Results

X-ray diffraction patterns are measured for the as-deposited, hydrogenated and de-hydrogenated states of samples 1, 2, 3, 4 and 5. As previously reported [3], in the as-deposited state Mg_yTi_{1-y} thin films have a hexagonal close-packed structure with an almost perfect Vegard's law dependence of the interplanar distances, while upon hydrogenation the alloys undergo phase transitions to a fluorite ($y < 0.87$) or a rutile ($y > 0.90$) structure (Fig. 1a).

In Fig. 1b the XRD patterns for sample 3 in the as-deposited, hydrogenated and de-hydrogenated states are shown. The only visible metallic peak is the 002 reflection arising from the hexagonal Mg–Ti alloy. In the as-deposited states of the Ti-rich compositions (samples 1, 2 and 3) a much smaller peak, similar to the 002 reflection for pure Ti ($2\theta = 38.42°$; hexagonal), is also present. This peak is not recovered after one hydrogenation/de-hydrogenation cycle and it is likely to be a satellite peak, rising from the coexistence of Ti and Mg domains with coherent boundaries [13]. The diffraction peaks at higher 2θ's are the 111 reflections of Pd and PdH_x, due to the palladium cap layer, in the metallic and hydrogenated states, respectively.

Fig. 2 shows the k^1-weighted background-subtracted EXAFS signal $\chi(k)$ for the as-deposited states of samples 1, 2, 3, 4 and 5, measured in He at room temperature. In all cases the measured edge-energy is equal to the edge-energy for the Ti reference (4966 eV), indicating a pure metallic state of the films. The inset in Fig. 2 shows the raw absorption data for sample 1, before background subtraction.

An example of fitted data is shown in Fig. 3 for sample 1 ($Mg_{0.53}Ti_{0.47}$). For all the samples the fits are optimized with $\Delta k = 3$–11 Å^{-1} and $\Delta R = 2.0$–3.4 Å. Table 2 summarizes the fit parameters obtained for all the compositions measured in the as-deposited state. The number of independent parameters

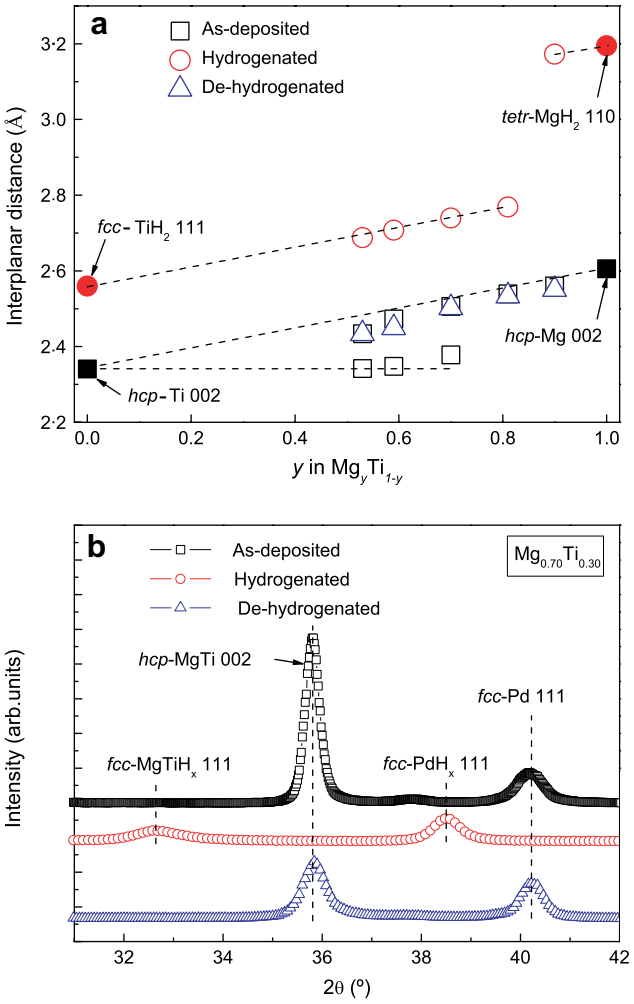

Fig. 1 – (a) Interplanar distances obtained from X-ray diffraction patterns for samples 1, 2, 3, 4 and 5 in the as-deposited (squares), hydrogenated (circles) and de-hydrogenated (triangles) states. Full squares and circles are literature values for Mg, Ti, MgH_2 and TiH_2. The dashed lines are a guide to the eye. (b) X-ray diffraction patterns for sample 3 in the as-deposited (squares), hydrogenated (circles) and de-hydrogenated (triangles) states.

used in the fit is in all cases lower than the maximum value set by the Nyquist theorem [21]. The coordination shell of Ti is composed of both Ti and Mg atoms. For all Mg_yTi_{1-y} thin films the total coordination number, given by the sum of the Ti–Ti and Ti–Mg coordination numbers, is close to the ideal value for an hexagonal geometry ($N = 12$). However, their relative amount changes with composition and is different from what would be expected for a completely random solid solution. From the Ti–Ti and Ti–Mg coordination numbers in a Mg_yTi_{1-y} alloy, the Chemical Short-Range Order (CSRO) parameter, s, can be calculated as follows [22]

$$s = 1 - \frac{N_{\mathrm{Ti\text{–}Mg}}}{(N_{\mathrm{Ti\text{–}Ti}} + N_{\mathrm{Ti\text{–}Mg}})y} \quad (1)$$

where $s = 0$ would correspond to a random distribution of Mg and Ti atoms, while $s = 1$ to a complete segregation into pure phases of Mg and Ti.

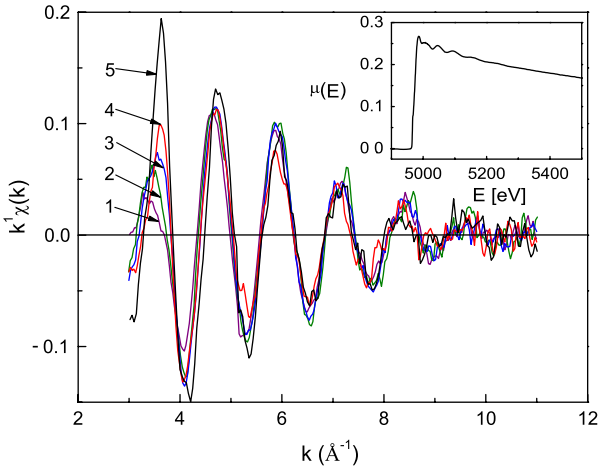

Fig. 2 – k^1-weighted background-subtracted $\chi(k)$ for samples 1, 2, 3, 4, and 5 (see Table 1) in the as-deposited states. All spectra are measured in He at room temperature. In the inset the absorption spectrum around the K-edge for sample 1 is shown.

The measured s values are reported in Table 2. The error in s is calculated assuming a ±10% error in the coordination numbers [23] while the error on the composition y, as measured with RBS, is negligible.

XANES spectra are continuously recorded during the hydrogenation and de-hydrogenation of the films. For all the compositions the Ti absorption edge is identical to the one measured for the reference Ti foil, indicating a purely metallic state of the as-deposited samples. Fully hydrogenated films are obtained by exposure of the as-deposited films to a 5% H_2/He mixture for few minutes at room temperature, the end of the hydrogenation being indicated by a stable XANES spectrum. Upon exposure to a 20% O_2/He mixture for ~1 h at

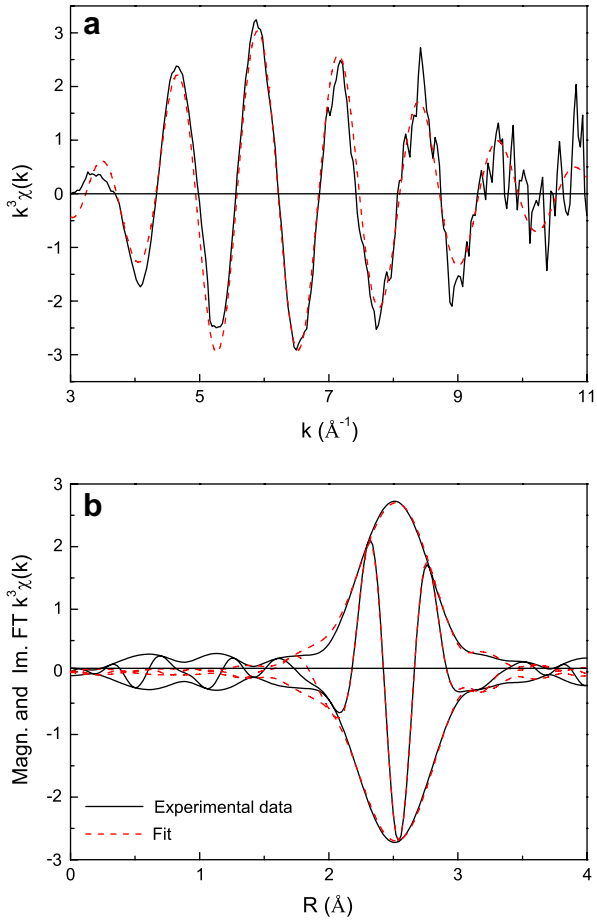

Fig. 3 – (a) k^1-weighted background-subtracted $\chi(k)$ and (b) Magnitude and Imaginary part of the phase-uncorrected Fourier transformed $\chi(k)$ for sample 1. The fit (dashed line) is optimized with $\Delta k = 3 - 11$ Å^{-1} and $\Delta R = 2.0 - 3.4$ Å.

Table 2 – Fit parameters for samples 1, 2, 3, 3a, 4 and 5 in the as-deposited states: coordination number N, Debye–Waller factor $\Delta\sigma^2$, distance R and inner potential correction ΔE_0.

Sample	Shell	N	$\Delta\sigma^2$ (10^{-3} Å^2)	R (Å)	ΔE_0 (eV)	y in Mg_yTi_{1-y}	CSRO, s
1 as-deposited	Ti–Ti	7.7	12.6	2.90	1.97	0.53	0.18 ± 0.05
	Ti–Mg	5.9	9.6	3.02	−1.02		
2 as-deposited	Ti–Ti	7.5	12.2	2.89	2.61	0.59	0.27 ± 0.05
	Ti–Mg	5.7	8.1	3.02	−0.31		
3 as-deposited	Ti–Ti	6.7	12.1	2.89	1.87	0.70	0.32 ± 0.04
	Ti–Mg	6.1	12.7	3.03	−0.47		
3a as-deposited	Ti–Ti	6.1	11.0	2.89	2.11	0.72	0.38 ± 0.04
	Ti–Mg	5.0	10.1	3.03	−0.17		
4 as-deposited	Ti–Ti	5.0	15.9	2.90	4.73	0.81	0.29 ± 0.03
	Ti–Mg	6.8	12.7	3.09	1.50		
5 as-deposited	Ti–Ti	5.0	18.3	2.93	2.24	0.90	0.35 ± 0.03
	Ti–Mg	7.1	8.9	3.09	1.76		
1 de-hydrogenated	Ti–Ti	6.8	13.4	2.89	3.44	0.53	0.16 ± 0.05
	Ti–Mg	5.5	10.3	2.96	1.52		
3a de-hydrogenated	Ti–Ti	6.4	13.8	2.89	3.42	0.72	0.33 ± 0.04
	Ti–Mg	5.9	10.6	3.03	0.61		
5 de-hydrogenated	Ti–Ti	5.8	22.1	3.00	2.88	0.90	0.37 ± 0.03
	Ti–Mg	7.7	8.2	3.11	3.30		

temperatures between room temperature and 100 °C, depending on film composition, the hydrogenated films release hydrogen and return to a metallic state. The comparison between the as-deposited and the de-hydrogenated metallic states, for three different compositions, is shown in Fig. 4, together with the fitted *s* values. The slight differences between the two metallic states (before and after hydrogenation) are mainly due to small changes in the coordination numbers and to an increase in the amount of disorder of the Ti–Ti shells.

4. Discussion

EXAFS data show that Mg_yTi_{1-y} thin films do not form random solid solutions and that a certain degree of atom rearrangement is already present in the as-deposited films. The amount of rearrangement does not depend strongly on composition: a chemical short-range order of $s \sim 0.3$ is found for a broad range of compositions. The slightly lower *s* values obtained for the Ti-richer compositions are probably due to the higher total deposition rates during sputtering (Table 1).

As shown in Fig. 5 the non-zero chemical short-range order leads to "spinodal-like" structures in the Mg_yTi_{1-y} alloys. Experimental evidence of such "spinodal-like" structures, characterized by compositional modulations with nanometer wavelengths [22], with similar values for the chemical short-range order parameters, has been reported both for amorphous [24] and crystalline [25] immiscible binary systems. The pictures in Fig. 5 are indicative of the degree of decomposition that occurs during films deposition and are generated via 3D Monte Carlo simulations, assuming only nearest-neighbor interactions and including periodic boundary conditions.

The chemical short-range order arises during the high-energy non-equilibrium deposition process, resulting in the partial segregation into Mg-rich and Ti-rich domains which is driven by the positive enthalpy of mixing of the two elements. Such ordering is also responsible for the fast kinetics and the exceptional robustness of these systems.

Comparison between the EXAFS spectra measured on the as-deposited and the de-hydrogenated films indicates a high structural reversibility of the Mg_yTi_{1-y} alloys, even at an atomic level. This result is particularly unexpected given the strong segregating effect of hydrogen on many Mg-based alloys, such as Mg–V [26], Mg–Sc [27], Mg–Y, Mg–La, Mg–Ce, and Mg–Gd [14]. Furthermore RBS results and the analysis of the absorption edge energies in the EXAFS spectra rule out the hypothesis that the stability upon hydrogen cycling of the Mg_yTi_{1-y} films, is due to the presence of impurities in the alloys or due to partial oxidation of the films.

The structural model developed to interpret the optical and electrical properties of $Mg_yTi_{1-y}H_x$ thin films [3] hypothesized the coexistence of Mg-rich and Ti-rich nanosized domains, within large coherent grains. This model is nicely and quantitatively confirmed by the positive chemical short-range order parameters measured by means of EXAFS (see Fig. 6).

As already suggested by Borsa et al. [3], once a spinodal coherent microstructure is formed upon film deposition, a key

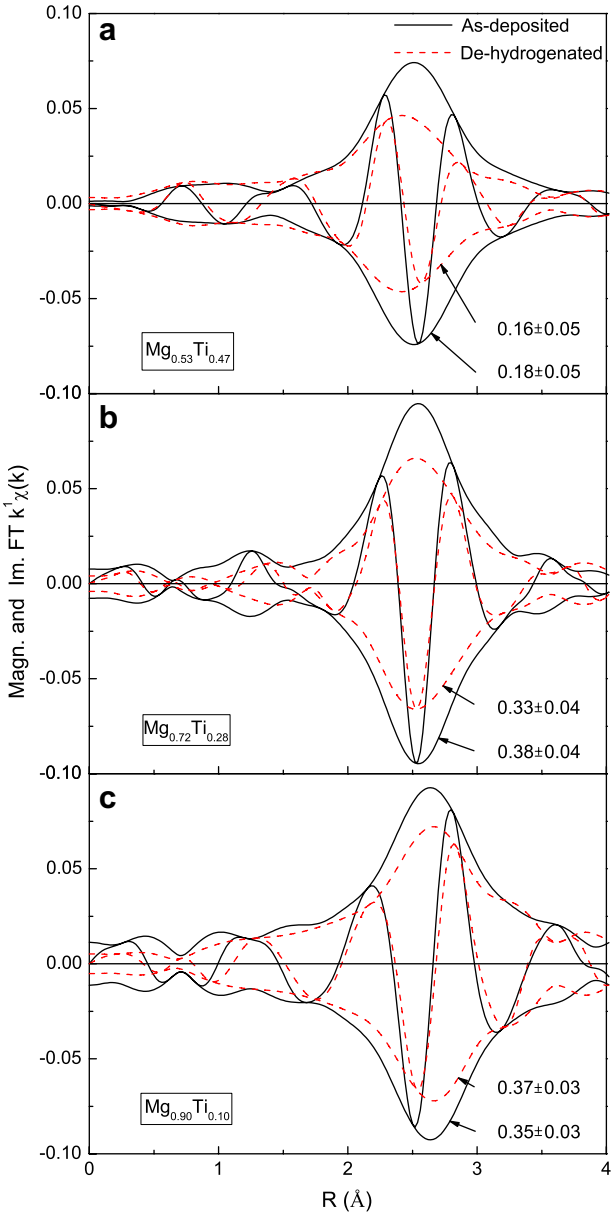

Fig. 4 – Magnitude and imaginary part of the phase-uncorrected Fourier transformed $\chi(k)$ for $Mg_{0.53}Ti_{0.47}$, $Mg_{0.72}Ti_{0.28}$ and $Mg_{0.90}Ti_{0.10}$ both in the as-deposited (solid line) and de-hydrogenated (dashed line) states. The numerical values indicate the chemical short-range order parameters obtained upon fitting.

ingredient for its stability is the similarity in the molar volumes of Mg (13.97 cm^3/mole) and TiH_2 (13.30 cm^3/mole). Ti has a more negative enthalpy of hydride formation than Mg, thus forming a hydride at lower pressures. Given the presence of chemical short-range order, the hydrogenation of our films proceeds in the following way (see Fig. 6): at very low hydrogen pressures a hydrogen solid solution forms in the Mg_yTi_{1-y} alloy producing a small expansion of the host lattice; with increasing pressure the Ti-rich parts hydrogenate and the internal lattice strains are substantially *released* by the coexistence of Mg and TiH_2 domains, thanks to the accidental equality of the molar volumes of the two components;

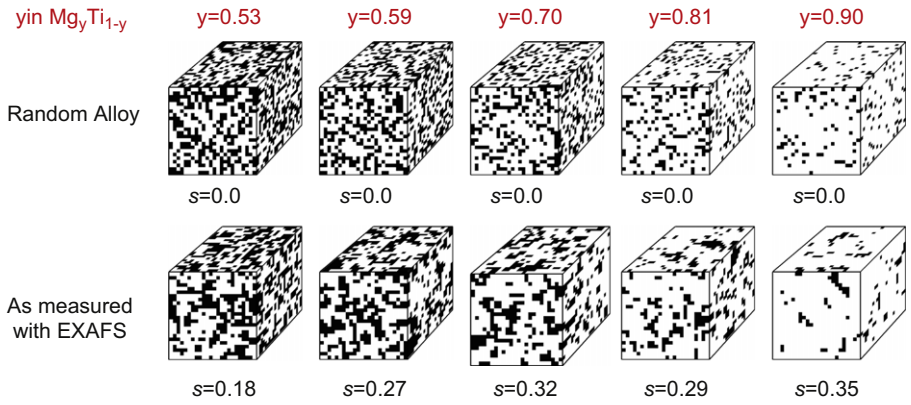

Fig. 5 – 3D-representation of Mg_yTi_{1-y} alloys with compositions as in samples 1, 2, 3, 4 and 5 and chemical short-range order parameters, s, as measured with EXAFS. For comparison the same compositions are shown for completely random distribution of Mg and Ti atoms (s = 0).

a further increase of hydrogen pressure eventually causes Mg-rich areas to form the di-hydride, MgH_2. The coherency with the fcc TiH_2 forces the MgH_2 to form in the fcc instead of the rutile phase. The same steps are followed in reverse order during unloading. As evidenced by XRD data the coherence of the alloy is maintained in the whole process.

Hydrogen atoms in a Mg_yTi_{1-y} alloy can occupy different tetrahedral Mg_jTi_{4-j} interstitial sites, with $0 \leq j \leq 4$. Taking into account the different site energies and including the effect of both short-range ordering and lattice distortions, Gremaud et al. [28] have successfully fitted the pressure-optical-transmission-isotherms measured by hydrogenography [29] on Mg_yTi_{1-y} thin films. The fitted values of the chemical short-range order parameter are in excellent agreement with the values measured in the present work with EXAFS and confirm the reversibility of these systems upon several hydrogen loading/unloading cycles.

Our measurements neatly confirm the structural picture which was deduced on the basis of the optical transition observed on hydrogenation. Note, that the thermodynamics of the hydrogenation of Mg is hardly affected [29]. This can be understood from the fact that the energy difference between the fcc and rutile phases is small [30]. The advantage for storage applications is that the fcc crystal structure allows for a favorable kinetics of hydrogen diffusion [31].

The nanoscale short-range deviations from a random solid solution measured in $Mg_yTi_{1-y}H_x$ thin films make it possible to understand quantitatively the hydrogen loading and unloading mechanisms. They also provide an interpretation of the non-trivial optical black state observed in the hydrogenated state of $Mg_yTi_{1-y}H_x$ thin films: the origin of this black state cannot be explained within a simple effective medium approximation. Recent *ab initio* density functional theory calculations by van Setten et al. [32] reproduce the observed

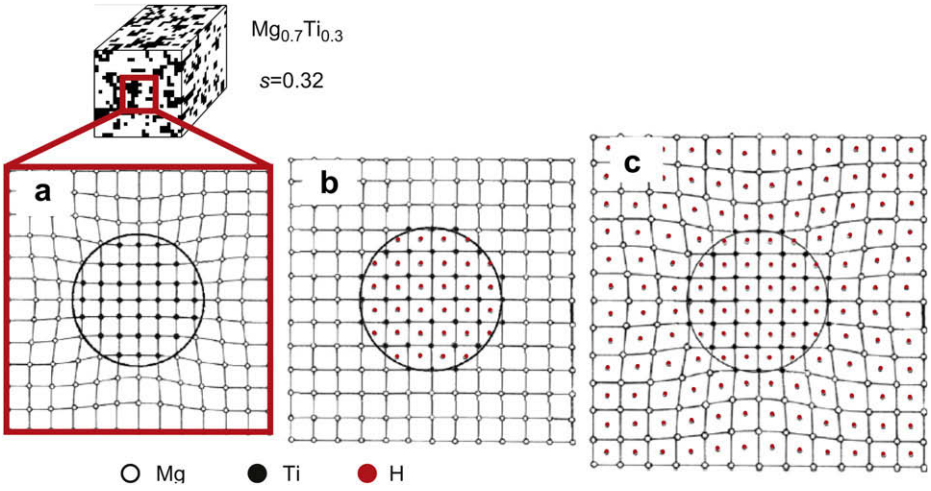

Fig. 6 – Enlargement of the $Mg_{0.7}Ti_{0.3}$ sample in Fig. 5, highlighting the "cluster-like" structure of the Mg_yTi_{1-y} thin films. (a) Schematic representation of a coherent crystalline grain consisting of a Mg and a Ti region; (b) the same crystalline grain after hydrogen uptake in the Ti sites, at low hydrogen pressures; (c) and in the fully hydrogenated state [3]. Note that the cartoons are only meant as an illustration of the stress-releasing intermediate state (b), when Ti has formed TiH_2 but Mg is still in its metallic state. (For interpretation of the references to colour in this figure legend, the reader is referred to the web version of this article.)

optical reflection and transmission spectra, taking into account a certain degree of ordering in the distribution of atoms in $Mg_yTi_{1-y}H_2$ super cells and including both inter-band and intra-band contributions to the dielectric function.

5. Conclusions

As standard X-ray diffraction techniques alone are inadequate for systems of immiscible elements [12], we combined XRD and EXAFS to study the local structure of Mg–Ti–H alloys. We show that in Mg_yTi_{1-y} thin films the distribution of Mg and Ti atoms is not random and that a certain level of local chemical segregation occurs, without affecting the long-range structural coherence of the film. The amount of segregation depends weakly on composition and is stable upon cycling with hydrogen. The ''spinodal-like'' distribution of atoms, suggested by Monte Carlo simulations, allows to understand the robustness of the system in terms of an accidental equality in the molar volumes of Mg and TiH_2. This kind of microstructure is of particular technological interest in the synthesis of new metastable materials, with high hydrogen storage capacities and fast hydrogen absorption and desorption kinetics. By applying the proper synthesis techniques one may thus aim to stabilize crystal structures not feasible according to basic thermodynamics. Our work shows that the possibilities to optimize the properties of hydrogen storage materials are more abundant than previously envisaged.

Acknowledgments

This work is financially supported by the Technologiestichting STW and the Stichting voor Fundamenteel Onderzoek der Materie (FOM) through the Sustainable Hydrogen Programme of Advanced Chemical Technologies for Sustainability (ACTS/NWO). The authors would also like to acknowledge D. Zajac, M. Slaman, J. H. Rector, H. Schreuders, S. de Man, A. Mijovilovich and E. de Smit for their technical and scientific support.

REFERENCES

[1] Niessen RAH, Notten PHL. Electrochemical hydrogen storage characteristics of thin film MgX (X = Sc, Ti, V, Cr) compounds. Electrochem Solid-State Lett 2005;10:A534–8.
[2] Borsa DM, Baldi A, Pasturel M, Schreuders H, Dam B, Griessen R, et al. Mg–Ti–H thin films for smart solar collectors. Appl Phys Lett 2006;88:241910.
[3] Borsa DM, Gremaud R, Baldi A, Schreuders H, Rector JH, Kooi B, et al. Structural, optical, and electrical properties of $Mg_yTi_{1-y}H_x$ thin films. Phys Rev B 2007;75:205408.
[4] Slaman M, Dam B, Pasturel M, Borsa D, Schreuders H, Rector JH, et al. Fiber optic hydrogen detectors containing Mg-based metal hydrides. Sens Actuators B Chem 2007;123:538–45.
[5] Baldi A, Borsa D, Schreuders H, Rector J, Atmakidis T, Bakker M, et al. Mg–Ti–H thin films as switchable solar absorbers. Int J Hydrogen Energy 2008;33:3188–92.
[6] de Boer FR, Boom R, Mattens WCM, Miedema AR, Niessen AK. Cohesion in metals: transition metal alloys. Amsterdam: North-Holland Physics; 1988.
[7] Mitchell T, Diplas S, Tsakiropoulos P, Watts JF, Matthew JAD. Study of alloying behaviour in metastable Mg–Ti solid solutions using Auger parameter measurements and charge-transfer calculations. Philos Mag A 2002;82:841–55.
[8] Vermeulen P, Niessen RAH, Notten PHL. Hydrogen storage in metastable Mg_yTi_{1-y} thin films. Electrochem Commun 2006;8:27–32.
[9] Vermeulen P, Niessen RAH, Borsa DM, Dam B, Griessen R, Notten PHL. Effect of the deposition technique on the metallurgy and hydrogen storage characteristics of metastable $Mg_yTi_{(1-y)}$ thin films. Electrochem Solid-State Lett 2006;9:A520–3.
[10] Liang G, Schulz R. Synthesis of Mg–Ti alloy by mechanical alloying. J Mater Sci 2003;38:1179–84.
[11] Vegard L. Die Konstitution der Mischkristalle und die Raumfüllung der Atome. Z Phys 1921;5:17–26.
[12] Ma E. Alloys created between immiscible elements. Prog Mater Sci 2005;50:413–509.
[13] Michaelsen C. On the structure and homogeneity of solid solutions: The limits of conventional X-ray diffraction. Philos Mag A 1995;72:813–28.
[14] Giebels IAME, Isidorsson J, Griessen R. Highly absorbing black Mg and rare-earth-Mg switchable mirrors. Phys Rev B 2004;69:205111.
[15] van der Sluis P, Ouwerkerk M, Duine PA. Optical switches based on magnesium lanthanide alloy hydrides. Appl Phys Lett 1997;70:3356.
[16] Kyoi D, Sato T, Rönnebro E, Kitamura N, Ueda A, Ito M, et al. A new ternary magnesium–titanium hydride Mg_7TiH_x with hydrogen desorption properties better than both binary magnesium and titanium hydrides. J Alloys Compd 2004;372:213–7.
[17] Kalisvaart W, Wondergem HJ, Bakker F, Notten PHL. Mg–Ti based materials for electrochemical hydrogen storage. J Mater Res 2007;22:1640–9.
[18] Vaarkamp M, Linders JC, Koningsberger DC. A new method for parameterization of phase shift and backscattering amplitude. Physica B 1995;208-209:159–60.
[19] Cook Jr JW, Sayers DE. Criteria for automatic X-ray absorption fine structure background removal. J Appl Phys 1981;52:5024.
[20] Koningsberger DC, Mojet BL, van Dorssen GE, Ramaker DE. XAFS spectroscopy; fundamental principles and data analysis. Top Catal 2000;10:143–55.
[21] Stern EA. Number of relevant independent points in x-ray-absorption fine-structure spectra. Phys Rev B 1993;48:9825–7.
[22] He JH, Ma E. Nanoscale phase separation and local icosahedral order in amorphous alloys of immiscible elements. Phys Rev B 2001;64:144206.
[23] Li GG, Bridges F, Booth CH. X-ray-absorption fine-structure standards: A comparison of experiment and theory. Phys Rev B 1995;52:6332–48.
[24] He JH, Sheng HW, Schilling PJ, Chien CL, Ma E. Amorphous structures in the immiscible Ag–Ni System. Phys Rev Lett 2001;86:2826–9.
[25] He JH, Sheng HW, Lin JS, Schilling PJ, Tittsworth RC, Ma E. Homogeneity of a supersaturated solid solution. Phys Rev Lett 2002;89:125507.
[26] Gonzalez-Silveira M, Gremaud R, Dam B, Griessen R, in preparation.
[27] Giebels Iame. Shining light on magnesium based switchable mirrors. Ph.D. thesis, VU University Amsterdam (2004), ISBN 90-9018547-X.
[28] Gremaud R, Baldi A, Gonzalez-Silveira M, Dam B, Griessen R. Chemical short-range order and lattice deformations in $Mg_yTi_{1-y}H_x$ thin films probed by hydrogenography. Phys Rev B 2008;77:144204.

[29] Gremaud R, Broeders C, Borsa DM, Borgschulte A, Mauron P, Schreuders H, et al. Hydrogenography: an optical combinatorial method to find new light-weight hydrogen storage materials. Adv Mater 2007;19:2813–7.
[30] Vajeeston P, Ravindran P, Kjekhus A, Fjellvåg H. Pressure-induced structural transitions in MgH_2. Phys Rev Lett 2002;89:175506.
[31] Conradi MS, Mendenhall M, Ivancic TM, Carl EA, Browning CD, Notten PHL, et al. NMR to determine rates of motion and structures in metal-hydrides. J Alloys Compd 2007;446–447:499–503.
[32] van Setten MJ, Er S, Brocks G, de Groot RA, de Wijs GA. 2008. arXiv:0804.0376.